Title: Impact of Medial Calcification on Arterial Mechanics and Haemodynamics

Authors: Pak-Wing Fok[1], Kun Gou[2], Brandon Myers[1], and Peter Lanzer[3]

Running Title: Impact of Medial Calcification on Haemodynamics

Corresponding Author:

Pak-Wing Fok,

412 Ewing Hall,

Department of Mathematical Sciences,

University of Delaware,

Newark,

DE 19716

pakwing@udel.edu

1 University of Delaware, Department of Mathematical Sciences, Newark, DE 19716, USA

2 Department of Computational, Engineering, and Mathematical Sciences, Texas A&M University – San Antonio, San Antonio, TX 78224, USA

3 Health Care Center Bitterfeld-Wolfen, Bitterfeld, Germany

Key Points Summary

- Medial Arterial Calcification (MAC) often occurs in aging arteries, promoted by diabetes mellitus and chronic kidney disease. Patients with advanced calcification may develop limb-threatening ischemia due to malperfusion.
- Through theoretical modeling and simulation, we find that calcified arteries experience a reduced flow rate because they present smaller lumen areas compared to healthy arteries.
- The systolic pressure decreases across calcified arteries whereas in healthy arteries, the systolic pressure usually increases. These findings have broad implications for localized detection of MAC.

Impact of Medial Calcification on Arterial Mechanics and Haemodynamics

Pak-Wing Fok, Kun Gou, Brandon Myers, and Peter Lanzer

Abstract

Medial Arterial Calcification (MAC) often occurs in aging arteries, promoted by diabetes mellitus and chronic kidney disease. Advanced MAC represents a frequent cause of chronic limb-threatening ischemia and limb amputation. Through a 1D haemodynamics simulation, we study how the mechanical properties of calcified arterial tissue and hydraulic resistance in the peripheral circulation jointly impact haemodynamics as MAC develops. We find that (i) there is a greater drop in systolic pressure across calcified arteries compared to healthy arteries, but this drop can be offset by greater peripheral resistance, provided left ventricular function is intact, (ii) both calcification and enhanced peripheral resistance lead to reduced flow rates, reduced peripheral perfusion, and peripheral tissue hypoxemia and (iii) pressurized calcified arteries present lumen areas that are smaller compared to healthy arteries, even though they are larger when unpressurized.

We also explore the effects of positive remodeling and elevated blood pressure. We find that a global luminal enlargement reduces the systolic and mean pressure drop across a calcified artery while increasing the mean outflow rate, thereby making a calcified artery behave more like a healthy one, hydrodynamically. Increasing the global pressure in a calcified artery further enhances the drop in systolic and mean pressure while increasing the mean outflow rate.

Our simulations suggest that the increased impedance in calcified arteries results from smaller *in-vivo* lumen areas. This can reduce the outflow rate, but the effect is complicated by arteriole closures, vessel geometry, and global pressure. These findings confirm previously reported observations of flow reduction in calcified arteries.

Introduction

Medial Arterial Calcification (MAC) is a vascular disorder, distinct from atherosclerosis, in which calcium phosphate (CaP) precipitates and crystalizes due to a breakdown of CaP homeostasis in the media (Lanzer, et al. 2021). The result is considerable mineralization and progressive destruction of the medial layer. In advanced MAC, extensive axial segments of an artery are calcified, and the calcifications eventually span the entire circumference, encasing the intima in rigid sheath. In contrast, atherosclerosis-associated calcification is spotty and occurs in the intima.

MAC occurs in aging arteries and is largely accelerated by diabetes mellitus (DM) and chronic kidney disease (CKD). In addition to calcification, intimal hyperplasia represents a second critical hallmark of MAC. Patients with advanced MAC, frequently diabetics, may eventually develop chronic limb-threatening ischemia which is often responsible for minor and major limb amputations: see Figure 1(a) for an example of ischemia-related necrosis in the finger. The hemodynamical mechanisms underlying the ischemia are not fully understood although some basic facts are known. For example, arteries stiffen due to calcification and intraluminal cross-sectional area may decrease (Fok and Lanzer 2018).

In this work, we study, *in-silico,* the haemodynamics of a large artery undergoing the joint effects of calcification, increased peripheral resistance, positive remodeling, and elevated pressure, which are all hallmarks of MAC. We propose that a drop in systolic pressure across an artery is a sufficient, but not necessary, condition of arterial calcification.

Figure 1(b) shows a time-pressure trace of a patient with MAC. Due to impaired pressure wave transmission, MAC arteries have a decreased systolic pressure at the outlet compared to the inlet resulting in an FFR (Fractional Flow Reserve) < 1. This contrasts with healthy arteries, where the systolic pressure usually amplifies as the pulse wave propagates downstream. Schematics for calcified and healthy arteries are shown in Figure 2. In MAC patients, the distal systolic pressure (Pd) has been observed to be lower than the central systolic pressure (Pa) so

that Pd/Pa < 1, whereas in a healthy artery, Pd/Pa > 1. It has been hypothesized that this marked reduction in the Pd/Pa ratio is an important indicator of MAC (Lanzer, et al. 2021) but this prediction lacks a rigorous theoretical justification.

Several studies have described how arterial stiffness and geometry affect the pressure pulse wave. Arterial stiffening generally augments both systolic pressure (Hashimoto 2022, Tsao 2014, Mitchell 2004) and pulse pressure (Chirinos 2019, Mitchell 2004). Systolic pressure often increases along large healthy arteries due to tapering and reflections from bifurcations (Lyle 2017, Van de Vosse 2011) with the result that brachial or femoral systolic pressures usually exceed central systolic pressures.

Multiple papers have reported the effect of age on arterial stiffness/geometry. It is well-documented (Lee 2010, Kamenskiy, et al. 2018) that arteries become stiffer and increase their diameters as they age. Arterial cross-sections of subjects of different ages often present different cardiovascular pathologies (Jadidi, et al. 2021), but older patients generally have arteries that have larger lumens and thicker walls. However, there are two important caveats. First, although a typical unpressurized healthy artery has a smaller lumen area than a typical unpressurized calcified artery, under physiological pressures, the healthy artery dilates more during systole than its calcified counterpart. Second, the studies in (Kamenskiy, et al. 2018) were performed on samples that had little intimal growth. Intima hyperplasia, if it occurs, will of course thicken the arterial wall, but it can also modify the lumen area in unexpected ways (Mukherjee, Mohammad Mirzaei and Fok 2024, Glagov, et al. 1987) causing either an increase or a decrease in lumen area depending on the extent of the growth.

Methods

Mathematical Model and Governing Equations

In this section, we present a model for 1D arterial blood flow. Such hemodynamic models are commonly used because the fluid flow is simplified (Alastruey, et al. 2009) and the resulting equations can be solved more quickly.

The 1D model makes several assumptions. First, components of the flow orthogonal to the axial direction are small enough to be neglected. Second, the artery is straight. Therefore, the lumen area $A(x,t)$, axial flow velocity $u(x,t)$ and blood pressure $p(x,t)$ are all functions of *x*, the position along the artery measured in centimeters and t, time measured in seconds. With these assumptions, we have

$$A_t + (uA)_x = 0 \tag{1}$$

$$u_t + uu_x = -\frac{p_x}{\rho} \tag{2}$$

$$p = f(A, B_0) \tag{3}$$

where ρ is the density of blood. The first two partial differential equations are derived from conserving the fluid's mass and momentum. In 1D haemodynamics, the final equation captures the artery's mechanical properties and is called a "tube law", often specified as an empirical relation. However, in our framework, the relationship between area and pressure is found numerically from a hyperelastic model where B_0 is the area of the unpressurized lumen. This is the main novelty in our method.

Specifically, we consider a hyperelastic annulus with thickness *h* and cross-sectional area B_0 in the stress-free state: see Figure 3(a). The mechanical properties of the annulus are dictated by a strain energy function that has already been parameterized for healthy and calcified arteries (Jadidi, et al. 2021). Assuming that the annulus is subject to an internal pressure *p* and the

external boundary is traction-free, the deformed lumen area *A* can be found: see the section *Mechanical Properties of Artery* below and the Appendix for further details.

In our model, the tube laws for healthy and calcified arteries do not need to be assumed. Rather, they are derived from published data sets such as (Jadidi, et al. 2021) and incorporated directly into our haemodynamics framework. The disadvantage is that evaluating the tube law becomes computationally costly. Our numerical method pre-computes an interpolant for the pressure-area relationship $p = f(A, B_0)$ for different reference cross-sectional areas B_0 along with derivatives of $f(A, B_0)$ with respect to A and B_0, which are needed in the blood flow model. The unpressurized lumen area B_0 changes along the artery because of tapering.

Vessel Geometry

We consider a straight tapered artery of length *L*. In the unpressurized, reference state, the lumen radius R(x) satisfies

$$R(x) = R_a\left(1 - \frac{x}{L}\right) + R_a.\zeta.\left(\frac{x}{L}\right) \qquad (4)$$

where R_a is the arterial radius at the inlet and ζ is the tapering factor. A tapering factor $\zeta = 1$ corresponds to no tapering while $\zeta = 0$ means the outlet radius is zero. The reference lumen area is then calculated as $B_0(x) = \pi R^2(x)$.

The thickness of the arterial wall *h* and the tapering factor ζ are chosen so that when the artery is subject to an internal pressure of $P_{in}(0) = 65.5\beta$ mmHg, the deformed diameters match closely with Figure 3 of (Raines, Jaffrin and Shapiro 1974), 20 – 60 cm from the Iliac bifurcation. Here, β is an amplification factor that is set to 1 for calibration and most of our results but can be increased to model the effects of elevated pressure. $P_{in}(t)$ is the inlet driving pressure (see *Inlet Boundary Conditions* below). Taking L = 40 cm, we found that *h* = 0.0744 cm and ζ = 0.75 produced a good match.

Initial Conditions

We inflate the entire artery with a pressure $P_{ext} = \beta \times P_{in}(0) = 65.5\beta$ mmHg. This yields a deformed lumen area for every value of x, which is used as the initial condition A(x,t=0). The initial fluid velocity is assumed to be zero everywhere: u(x,0) = 0. Finally, P_b is the pressure at the branching point in the peripheral vasculature, and we set its initial condition as $P_b(t=0) = P_{ext}$: see Figure 4. Because the entire femoral artery is initially at the same pressure P_{ext}, we also have $P_{out}(t=0) = 65.5\beta$ mmHg.

Inlet Boundary Conditions

Using Matlab's `csaps.m` function, we constructed a smoothing spline approximation to the time-pressure data from the superficial femoral artery in Figure 7 of (Raines, Jaffrin and Shapiro 1974). This procedure defined the function $P_{in}(t)$. The data was extended periodically from $0 < t < 1$ to $-1 < t < 2$ before fitting the spline so that $P_{in}(t)$ over [0,1] was identical to $P_{in}(t)$ over [1,2]. To account for an elevated inlet pressure, $P_{in}(t)$ is scaled by an amplification factor β.

Outlet Boundary Conditions

Windkessel models are commonly used to describe blood flow, representing a complex cardiovascular system such as a heart chamber or an artery with a single compartment (Olufsen and Nadim 2004, L. Formaggia, et al. 2006). Although they have been used as stand-alone compartment models, they can also describe the terminal conditions in spatially resolved blood flow simulations. Windkessel models are composed of electrical components such as resistors, capacitors, and inductors that are tuned to imitate the viscous dissipation, vessel compliance and fluid inertia in a vascular network.

To simulate the post-arterial peripheral circulation, we consider a Windkessel model that has been structured to qualitatively imitate arborization: see Figure 4. The main femoral artery attaches to a single resistor with resistance R_0, which is, in turn, attached to N smaller "arterioles" in parallel. Each arteriole is composed of a resistor with resistance R and a capacitor with capacitance C. The post-peripheral pressure is set to $P_0 = 0$ mmHg. If the total resistance

and capacitance of the N arteries are R_T and C_T respectively, then the N arterioles can be replaced with a single parallel RC combination, resulting in a simple 3-component Windkessel element: two resistors with resistances R_0 and R_T and a capacitor with capacitance C_T. In the *Numerical Methods* section below we describe how R_T and C_T are modified when *j* of the arterioles are closed.

Note that the parallel resistor/capacitor components in Figure 4 do not represent single vessels. When Windkessel elements are used to provide terminal boundary conditions, their parameters are tuned to match hemodynamic data: see the *Numerical Methods* section below for details. Individual components may be thought of as collections of vessels with a total effective resistance and capacitance.

After using Kirchhoff's laws and the definition of the forward characteristic W_f (see the Appendix for the formulation of eqs. (1)-(2) in terms of characteristic variables W_f and W_b), we obtain the following system of outlet conditions at x = L:

$$C\frac{dP_b}{dt} + \frac{P_b}{R} = Q + \frac{P_0}{R} \tag{5}$$

$$f(A(L,t), B_0(L)) - P_b = QR_0 \tag{6}$$

$$A(L,t)\, W_f(L,t) = Q(L,t) + Av(A(L,t), B_0) \tag{7}$$

where

$$v(A, B_0) = \int_{B_0}^{A} \frac{c(A', B_0)}{A'}\, dA' \tag{8}$$

In eqs. (5)-(7), P_b is the pressure to the right of the first resistor in Figure 4 and $Q = u \times A$ is the flow rate at x=L. In eq. (8), *c* is the pulse wave speed and is defined mathematically in the

Appendix. Therefore, at the outlet we have 3 equations for the 3 unknown quantities P_b, A, and Q.

Mechanical Properties of Artery

We give an explicit formula for the tube-law f(A,B_0) through hyperelastic modeling of a pressurized annular cylinder with thickness *h*, following (Jadidi, et al. 2021). This model assumes that the arterial wall behaves mechanically like a neo-Hookean solid, but reinforced with two families of collagen fibres oriented at angles ϕ and -ϕ with respect to the circumferential unit vector:

$$f(A,B_0) = -\int_{\sqrt{B_0/\pi}}^{\sqrt{B_0/\pi}+h} \frac{\mathrm{dS}}{S\alpha^2}\left[\mu\left(\frac{1}{\alpha^2}-\alpha^2\right)+4k_1E\,e^{k_2E^2}\left(\frac{1-2c_1-c_2}{\alpha^2}-\alpha^2(c_1+c_2\cos^2\phi)\right)\right] (9)$$

where

$$E(S;A,B_0) = c_1\left(\frac{1}{\alpha^2}+\alpha^2+1\right)+c_2(\alpha^2\cos^2\phi+\sin^2\phi)+\frac{(1-3c_1-c_2)}{\alpha^2}-1,$$

$$\alpha = \alpha(S;A,B_0) = \frac{\sqrt{S^2+(A-B_0)/\pi}}{S},$$

and $c_1 = 2\,\kappa_{op}\kappa_{ip}$ and $c_2 = 2\,\kappa_{op}(1-2\kappa_{ip})$. Details of the derivation are given in the Appendix. The parameter ϕ (in radians) represents the fibre angle. μ, k_1 and k_2 are strain energy coefficients and κ_{op} and κ_{ip} are parameters quantifying fibre dispersion. The authors of (Jadidi, et al. 2021) mechanically tested femoral arterial tissue taken from deceased subjects that exhibited various cardiovascular pathologies. Through this testing, numerical values of the 6 parameters ϕ, μ, k_1, k_2, κ_{op} and κ_{ip}were found for both healthy and calcified arteries and incorporated into our simulation.

For a healthy artery, we used the parameters from Patient 2 of the paper, who exhibited no pathologies. For a severely calcified artery, we used the parameters from Patient 14 who was a former smoker and exhibited coronary artery disease, dyslipidemia, and hypertension. The arteries of Patient 14 were classified as having severe calcification and a moderately thickened intima. Table 1 shows the values of the 6 parameters. The subscripts 'H' and 'C' are used to differentiate between healthy and calcified arteries respectively.

In addition to predicting the behavior of healthy and severely calcified arteries, we also simulate mildly and moderately calcified vessels. For these cases, we calculate the mechanical parameters using interpolation:

$$\begin{aligned} \kappa_{ip} &= (1-\lambda)\kappa_{ip,H} + \lambda\kappa_{ip,C} \\ \kappa_{op} &= (1-\lambda)\kappa_{op,H} + \lambda\kappa_{op,C} \\ k_1 &= (1-\lambda)k_{1,H} + \lambda k_{1,C} \\ k_2 &= (1-\lambda)k_{2,H} + \lambda k_{2,C} \\ \mu &= (1-\lambda)\mu_H + \lambda\mu_C \\ \phi &= (1-\lambda)\phi_H + \lambda\phi_C \end{aligned} \tag{10}$$

For mildly calcified tissue, we take $\lambda = 0.15$ and for moderately calcified tissue, we take $\lambda = 0.30$.

In Figure 3(b), we plot the pressure-area curve $p = f(A,B_0)$ for healthy and calcified arteries. We see that a calcified artery dilates much less than a healthy artery, under the same pressure. Although at p=0, the calcified artery has a larger lumen, when the pressure in both arteries is increased, the healthy artery dilates much more since it is more compliant. This difference in behavior between elastic and calcified arteries has important consequences for their transport properties.

Numerical Methods

Eqs. (1) – (3) are solved in their characteristic form using a first order upwind scheme with $f(A,B_0)$ defined by eq. (9). At the inlet, the pressure is defined by $P_{in}(t)$ and at the outlet, $P_{out} = f(A(L,t),B_0(L))$ evolves through eqs. (5) – (7). We solve for $0 < t < 2$, finding that the flow requires about 1 second to become periodic, starting from a solution at rest. We ignore the solutions for $0 < t < 1$ and record the velocity $u(x,t)$ and lumen area $A(x,t)$ for $1 < t < 2$ and $0 < x < L$. Pressure and flow rate are computed as $p(x,t) = f(A(x,t),B_0(x))$ and $Q(x,t) = u(x,t) \times A(x,t)$. As a check, the governing equations were integrated over longer periods of time and the solutions for $1 < t < 2$ were not significantly different than the ones for $2 < t < 3$ (for example).

To determine the resistances and capacitances of the Windkessel elements in a healthy artery, we used simulated data from Figure 7 of (Raines, Jaffrin and Shapiro 1974) which illustrates pressure waveforms at the common iliac, external iliac, superficial femoral and distal popliteal arteries. Matlab's `fmincon.m` optimization function was used to find the 3 Windkessel parameters C_T, R_0, and R_T, that best-fit the pressure waveform from the *distal popliteal* artery. The capacitance C_T was constrained to lie between 0 and 30 cm^3/mmHg and R_0, and R_T were constrained to lie between 0 and 30 mmHg s/cm^3. This approach yielded the optimal (C_T, R_0, R_T) shown in Table 2.

We adopt the following procedure to model MAC-associated luminal narrowing and closure in peripheral vessels. An increase in peripheral resistance, along a decrease in compliance, is modeled by taking $R \to \infty$ and $C = 0$ for a subset of the arterioles in Figure 4. If $0 \leq j < N$ represents the number of vessels that are closed, a simple calculation reveals that the total resistance and capacitance of the Windkessel elements are

$$R_1 = \frac{R_T}{1 - s}$$

$$C_1 = C_T(1 - s)$$

where s = j/N is the fraction of closed vessels. While an intact peripheral vasculature is parameterized by (C_T, R_0, R_T), a MAC-afflicted peripheral vasculature is described by Windkessel parameters (C_1, R_0, R_1). Although the value of *N* is unknown, we can nevertheless simulate progressive obstruction in the periphery by allowing *s* to increase continuously from 0 to 1.

Results

Simulation Results.

The most important factor to consider in a MAC artery is wall stiffening due to calcification. In addition, MAC is often accompanied by progressive closure of arterioles, resulting in an enhanced peripheral resistance. Although both stiffening and peripheral resistance can occur concurrently, a benefit to using simulation to explore MAC is that these changes can be studied independently. First, we gain insight into how an artery's mechanical properties and its peripheral resistance impact local haemodynamics. Then we consider additional physiological changes to the hemodynamic environment and artery due to a patient's age. The two that we will consider are elevated blood pressure and positive remodeling of the arterial wall. For convenience, we introduce the quantities

$$\Delta_s = \text{Systolic pressure at outlet - Systolic pressure at inlet} \quad (11)$$

$$\Delta_m = \text{Mean pressure at outlet - Mean pressure at inlet} \quad (12)$$

which we study extensively in our simulations.

Effect of pure calcification.

Figure 5 shows how increasing arterial stiffness affects pressure, flow rate and lumen area. All arterioles in the peripheral circulation are kept open. The femoral arteries in each case have identical dimensions in the unpressurized state and are driven by the same inlet pressure. Solid blue curves correspond to quantities recorded at x = 0 while solid red curves correspond to quantities recorded at the end of the artery, x=L. Dashed lines represent time averages over $1 < t < 2$.

As an artery becomes stiffer, modeled by an increase in λ, the outlet systolic pressure drops resulting in $\Delta_s < 0$. The difference in mean pressure increases resulting in Δ_m becoming more negative. While the flow rate at the inlet lags that of the outlet in the healthy artery, they become more in-phase as the artery stiffens. The area of the arterial lumen shrinks, resulting in an overall decrease in the flow rate as indicated in Figure 5(e) – (h). The dilatory response of the lumen to pressure pulses is also reduced as λ increases: a severely calcified vessels exhibits very little pulsatility. While a healthy vessel has a mean flow rate of about 18 cm^3/s, this drops to about 12 cm^3/s for a severely calcified artery. Peak flow rates at the outlet drop from about 40 cm^3/s to 20 cm^3/s.

Effect of calcification and arteriole closures.

We now explore the effect of independently increasing stiffness in the main vessel *and* increasing resistance in the peripheral circulation. Again, all arteries are geometrically identical at zero pressure and are driven by the same inlet pressure waveform. We present our results in the form of colormaps. For each flow metric, we compute its functional dependence on λ (degree of calcification) and *s* (fraction of arteriole closures).

In Figure 6(a), we see that as the vessel stiffens, the outlet systolic pressure drops and Δ_s becomes more negative. For severely calcified vessels, pressure drops as large as 50 mmHg are possible. This is accompanied by an increase in Δ_m in Figure 6(b), indicating an increase in the impedance of the vessel. On the other hand, as more arterioles shut down, the systolic and mean pressures at the outlet increase, resulting in a rise in Δ_s and Δ_m. Overall, pressure changes due to calcification can be offset by closing arterioles.

Figure 6(c) shows that the outflow rate decreases when more arterioles close, or when the main vessel becomes more calcified. In Figure 6(d) mean flow rates drop from about 18 cm^3/s, for a healthy vessel with no closures, at $(\lambda,s) = (0,0)$, to about 4 cm^3/s, for a severely calcified vessel with a high fraction of closures when $(\lambda,s) = (1, 0.85)$. Although not shown in Figure 6, for a

fixed number of arterioles, as the vessel becomes more calcified, the outlet flow rates become more synchronized with the inlet flows similar to the ones shown in Figure 5(e) – (h). In severely calcified vessels, the outlet flow rate responds almost instantly to changes in the inlet. Finally, Figure 6(e, f) shows how the lumen areas at the inlet and outlet are impacted by vessel stiffening and progressive arteriole shutdown. Lumen areas are unaffected by arteriole closures but quickly decrease as calcification progresses.

One can imagine that the state of a healthy artery undergoing both calcification and arteriole closures is represented by a trajectory starting at (λ, s) = (0,0). Such an artery could take multiple pathways as indicated in Figure 6(a). In pathway A, calcification and closures occur at the same rate and Δ drops slightly before recovering. In B, substantial calcification occurs before rapid arteriole closures resulting in a steep drop in Δ_s and an eventual recovery. Finally in C, rapid arteriole closures occur before substantial calcification. In this case, Δ_s increases and then decreases. The same arguments can be applied to any of the flow metrics shown in Figure 6. The overall effect of MAC on haemodynamics depends on the competition between calcification rate and closure rate of arterioles.

Effect of calcification, increased mean pressure, and vessel remodeling.

So far, we have only explored the effect of stiffening without considering changes in pressure, or remodeling of the main artery. Generally, MAC arteries are larger and subject to higher pressures because MAC patients tend to be older.

In our simulations, thickening the wall does not have a significant effect on the outlet pressure. When the arterial wall is thickened by about 20%, from h = 0.074 cm to 0.090 cm, the pressure-area function p = $f(A,B_0)$ is not significantly affected and there is a negligible effect on the haemodynamics, irrespective of degree of calcification. On the other hand, Figure 7 shows the effect of positive remodeling on healthy and calcified arteries, simulated by increasing the unpressurized radius R_a. An increase in lumen size (dashed curves) affects $f(A,B_0)$ because the

same pressure results in a larger lumen area. Increasing the unpressurized inlet radius R_a from 0.15 cm to 0.17 cm increases the systolic pressure at the outlet by about 10 mmHg in both healthy and calcified cases. Note that the tapering factor $\zeta = 0.75$ remains unchanged and R_b increases in accordance with eq. (4). When the lumen area is increased *and* the wall is thickened, the overall effect is the same as enlarging the lumen without thickening the wall.

Next, we study the effect of calcification occuring concurrently with luminal enlargement, and calcification occuring concurrently with pressure elevation, while keeping the closure fraction *s* fixed. Because simulations are initialized with a hydrostatic pressure $P_{ext} = \beta\, P_{in}(t=0)$, increasing α increases the pressure throughout the artery at t=0 and elevates the time-averaged pressure at every spatial point in the vessel. Therefore, luminal enlargement and pressure elevation are modeled by increasing R_a and α respectively. In Figure 8 we see that Δ_s, Δ_m, and mean flow rate all increase as R_a increases for fixed λ. The effect of positive remodeling is to increase the pressure and flow rate at the outlet, thereby counteracting the pressure and flow rate changes induced by calcification alone.

In Figure 9, we see that Δ_s and Δ_m both decrease as α increases for fixed λ. These results are consistent with physical intuition. The terminal pressure in Figure 4 is pinned at $P_0 = 0$ and when α increases, the mean inlet pressure also increases, resulting in an increase in the mean of $P_{in}(t) - P_0$. The enhanced pressure drop must occur over both the main artery and the peripheral resistance so $P_{in} - P(L,t)$ would increase. A greater pressure drop induces a larger mean flow as shown in Figure 9(c). Overall, increasing the pressure throughout the artery enhances the pressure drop across the artery and augments the mean flow.

Discussion

Our simulations reveal that because calcified arteries are stiffer than healthy arteries, they expand less and present a smaller cross-sectional lumen area when subjected to the same internal pressure. MAC reduces the functional (pressurized) lumen area, increasing the

impedance of the vessel. Therefore, calcified arteries present a lower flow rate for a given pressure difference than a healthy artery with the same unpressurized dimensions. As a result, transport of oxygenated blood into the peripheral circulation is reduced, likely contributing to decreased oxygen supply into the dependent peripheral tissues. Theoretically, calcification could be detected by monitoring changes in systolic intraarterial pressure along the artery in question. Our computations support previous empirical observations on flow reduction in calcified arteries (Jinnouchi, et al. 2021, Lanzer, et al. 2021)

However, in practice, MAC is often accompanied by progressive, diffuse obliteration of peripheral microcirculation, and an enlargement of the unpressurized lumen. Our simulations suggest that both effects *increase* the systolic pressure at the arterial outlet, thereby opposing the changes caused purely by calcification. In other words, increased peripheral resistance and positive remodeling can obscure the signature of calcified arteries, making it difficult to detect purely by intraarterial pressure measurements. We also studied the behavior of the flow rate. Calcification and obliteration of the microcirculation, common consequences of MAC, both reduce the flow rate while luminal enlargement and elevated blood pressure, common consequences of aging, increase it. The effects of increasing stiffness, arteriole closures, positive remodeling, and increasing inlet pressure are summarized in Table 3. Note that outlet systolic pressure increases with α even though Figure 9(c) shows that Δ_m decreases with α. There is no contradiction since the inlet pressure increases more quickly compared to the outlet pressure.

A robust feature of our simulations is that as arteries become stiffer, they synchronize their inlet and outlet flow rates as shown in Figure 5(h). Severely calcified arteries behave like stiff tubes that barely deform in response to physiological pressures. For infinitely stiff tubes, conservation of mass dictates that the flow rate at $x=0$ must exactly equal the flow rate at $x=L$.

Surprisingly, we find that a thickening of the arterial wall does not greatly impact the haemodynamics. When we increased the wall thickness by 20%, the pressure-area relationship and the resulting haemodynamics were not substantially affected. To see significant differences

in the pressure-area curve over the range 0 – 200 mmHg, we found that the wall thickness had to be increased by about 100% or more, i.e. its thickness had to at least double.

The qualitative behavior of the haemodynamics can also be understood by using a voltage divider analogy from electrical circuits. While the analogy is only valid for the linearized form of eqs. (1)-(3), it provides a quick and intuitive understanding of our results. The main artery and the peripheral microcirculation can be represented using two impedance components in series with complex impedances Z_1 and Z_2 respectively. Two physiological changes are apparent as MAC develops in an artery: vessel stiffening and a progressive shutdown of arterioles in the periphery. Both processes increase the associated impedance, with the outlet pressure (P_{out}) and flow rate (Q) determined by

$$P_{\text{out}} = Re\left[\frac{P_{\text{in}}\, Z_2}{Z_1 + Z_2} + \frac{P_0\, Z_1}{Z_1 + Z_2}\right], \tag{11}$$

$$Q = Re\left[\frac{(P_{\text{in}} - P_0)}{Z_1 + Z_2}\right], \tag{12}$$

where Re[.] denotes the real part of a complex number, P_{in} is the inlet pressure, and P_0 is the terminal pressure. By eq. (11), if the artery stiffens without an increase in peripheral resistance, Z_1 increases while Z_2 remains constant, driving P_{out} closer to P_0. If the peripheral resistance increases without an increase in stiffness, Z_2 increases while Z_1 remains constant, driving P_{out} closer to P_{in}.

In eq. (12), any increase in Z_1 or Z_2 decreases the flow rate Q. Unlike pressure, for the flow rate, the impedances do not compete against each other. Instead, any increase in peripheral resistance *or* arterial stiffness decreases the mean flow rate. This was evident from Figure 6(c, d): the outflow decreases when more arterioles close off or when the main vessel becomes more calcified. Although the expressions for P_{out} and Q in (11) and (12) are underpinned by a

linear pressure/flow-rate response, they qualitatively agree with our fully nonlinear haemodynamics simulations.

It has been reported that calcified arteries have a smaller opening angle than healthy arteries (Kamenskiy, et al. 2018). Our simulations do not account for arterial opening angles since the arteries are always stress-free when *p=0*. Nevertheless, they already illustrate significant hemodynamical differences between healthy vs calcified arteries. When calcified arteries and healthy arteries have different opening angles, the stress distributions within their walls will be different, and their mechanical responses will also be different. How these changes subsequently modify the haemodynamics remains an important open question.

Our simulations describe how haemodynamics in the femoral artery is affected when it calcifies, in the absence of intimal hyperplasia or atherosclerosis. When atherosclerosis and MAC interact with each other, their joint effect on the haemodynamics is complex. Our model has neglected growth in the intima, focusing instead on remodeling in the media. Furthermore, we have treated the arterial wall as spatially homogeneous when in fact the intima, media, and adventitia have distinct mechanical properties (Fok and Gou, 2020; Fok, 2016). Growth in the intima can increase *or* decrease the lumen area (Mohammad Mirzaei and Fok 2020, Glagov, et al. 1987) as well as change the mechanical properties of the arterial wall. Future work should focus on modeling intimal thickening, media remodeling, and calcification using a multi-layered approach (Fok, 2016). To achieve a more complete understanding of MAC, one must address their combined effects on the mechanical response of the artery and the local haemodynamics.

The ankle-brachial index (ABI) - calculated as the ratio of the systolic pressure in the ankle to the systolic pressure in the arm - is often used to classify patients as either having MAC (ABI > 1.4) or not (ABI < 1.4); the cut-off value of 1.4 is an internationally recognized marker (Marius, et al. 2014, Aboyans, et al. 2012). When using a pressure cuff to measure ABI, the systolic pressure is measured as the minimum pressure required to close the artery and shut down bloodflow. However, a greater pressure is required to close a calcified artery in the leg: as a result, the cuff

pressure will exceed the actual intraarterial pressure if measured in the calcified arteries. The enhanced closing pressure arises because of the mechanical properties of a stiffer artery rather than an elevated systolic pressure. In fact, our simulations indicate that the outlet systolic pressure in a calcified femoral artery should not be elevated but *reduced*.

Currently, this hypothesis has not been tested in the clinical setting. However, we have taken blood pressure readings in a small (30) cohort of patients using an arteriograph (Tensiomed, Budapest, Hungary). The device measures the brachial pressure and infers the central pressure. We found that patients with ABI > 1.4 were more likely (14 out of 21 patients) to have a central systolic pressure that exceeded brachial systolic pressure than patients with ABI < 1.4 (5 out of 9 patients). However, these results are only weakly related to our hypothesis because an elevated ABI is an indicator of calcification in the arteries of the *lower extremities* and assumes that brachial arterial calcification is negligible.

Acknowledgements

Figure 2 was created using the University of Delaware's institutional BioRender license. KG was funded by a Texas A&M University-San Antonio Research Council Grant.

Bibliography

Aboyans, V., M. H. Criqui, P. Abraham, and M. A. et al. Allison. 2012. "Measurement and Interpretation of the Ankle-Brachial Index: A Scientific Statement From the American Heart Association." *Circulation* 126 (24).

Alastruey, J., K. H. Parker, J. Peiro, and S. J. Sherwin. 2009. "Analysing the pattern of pulse waves in arterial networks: a time-domain study." *Journal of Engineering Mathematics* 64: 331 - 351.

Chirinos, J.A., Segers, P., Hughes, T. and Townsend, R. 2019. "Large-artery stiffness in health and disease: JACC state-of-the-art review." *Journal of the American College of Cardiology* 74 (9): 1237-1263.

Fok, P.-W., and P. Lanzer. 2018. "Media sclerosis drives and localizes atherosclerosis in peripheral arteries." *PLoS one* 13 (10): e0205599.

Fok, Pak-Wing. 2016. "Multi-Layer Mechanical Model of Glagov Remodeling in Coronary Arteries: Differences between In-Vivo and Ex-Vivo Measurements." *PLoS ONE* 11 (7): e0159304.

Fok, Pak-Wing, and Kun Gou. 2020. "Finite element simulation of intimal thickening in 2D multi-layered arterial cross sections by morphoelasticity." *Computer Methods in Applied Mechanics and Engineering* 363: 112860.

Fok, Pak-Wing, and Rebecca Sanft. 2017. "A biochemical and mechanical model of injury-induced intimal thickening." *Mathematical Medicine and Biology* 34 (1): 77 - 108.

Formaggia, L, D Lamponi, M Tuveri, and A. Veneziani. 2006. "Numerical modeling of 1D arterial networks coupled with a lumped parameters description of the heart." *Computer Methods in Biomechanics and Biomedical Engineering* 9: 273 - 288.

Formaggia, Luca, Danielle Lamponi, and Alfio Quarteroni. 2003. "One-dimensional models for blood flow in arteries." *Journal of Engineering Mathematics* 47: 251 - 276.

Glagov, Seymour, Elliot Weisenberg, Christopher K. Zarins, Regina Stankunavicius, and George J. Kolettis. 1987. "Compensatory Enlargement of Human Atherosclerotic Coronary Arteries." *The New England Journal of Medicine* 316 (22): 1371 - 1375.

Hashimoto, J. 2022. "Arterial stiffness and pulsatile hemodynamics in coronary artery disease and other forms of atherosclerotic vascular diseases." In *Textbook of Arterial Stiffness and Pulsatile Hemodynamics in Health and Disease*, 621-635. Academic Press.

Jadidi, Majid, Selda Sherifova, Gerhard Sommer, Alexey Kamenskiy, and Gerhard A. Holzapfel. 2021. "Constitutive modeling using structural information on collagen fiber direction and dispersion in human superficial femoral artery specimens of different ages." *Acta Biomaterialia* 461-474.

Jaminon, Armand, Koen Reesink, and Leon Schurgers. 2019. "The Role of Vascular Smooth Muscle Cells in Arterial Remodeling: Focus on Calcification-Related Processes." *International Journal of Molecular Sciences* 20 (5694).

Jinnouchi, Hiroyuki, Yu Sato, Rahul R. Bhoite, Salome H, Kuntz, Atsushi Sakamoto, Matthew Kutyna, Sho Torii, et al. 2021. "Intravascular imaging and histological correlates of medial and intimal calcification in peripheral artery disease: Calcification of PAD by OFDI and IVUS." *Eurointervention* e688.

Kamenskiy, Alexey, William Poulson, Sylvie Sim, Austin Reilly, Jiangtuo Luo, and Jason MacTaggart. 2018. "Prevalence of Calcification in Human Femoropopliteal Arteries and its Association with Demographics, Risk Factors, and Arterial Stiffness." *Arteriosclerosis, Thombosis and Vascular Biology* e48 - e57.

Lanzer, Peter, Fadil M. Hannan, Jan D. Lanzer, Jan Janzen, Paulo Raggi, Dominic Furniss, Mirjam Schuchardt, et al. 2021. "Medial Arterial Calcification." *Journal of the American College of Cardiology* 78 (11).

Lee, H. Y. and Oh, B. H. 2010. "Aging and arterial stiffness." *Circulation Journal* 74 (11): 2257-2262.

Lyle, A.N. and Raaz, U. 2017. "Killing me unsoftly: causes and mechanisms of arterial stiffness." *Arteriosclerosis, thrombosis, and vascular biology* 37 (2): e1-e11.

Marius, R.A., L. Iliuta, S.M Guberna, and C. Sinescu. 2014. "The role of ankle-brachial index for predicting peripheral arterial disease." *Maedica* 295 (3): 295.

Mitchell, G.F., Parise, H., Benjamin, E.J., Larson, M.G., Keyes, M.J., Vita, J.A., Vasan, R.S. and Levy, D. 2004. "Changes in arterial stiffness and wave reflection with advancing age in healthy men and women: the Framingham Heart Study." *Hypertension* 43 (6): 1239-1245.

Mohammad Mirzaei, Navid, and Pak-Wing Fok. 2020. "Simple model of atherosclerosis in cylindrical arteries: impact of anisotropic growth on Glagov remodeling." *Mathematical Medicine and Biology* 38 (1): 59 - 82.

Muhire, G., Iulita, M.F., Vallerand, D., Youwakim, J., Gratuze, M., Petry, F.R., Planel, E., Ferland, G. and Girouard, H.,. 2019. "Arterial stiffness due to carotid calcification disrupts cerebral blood flow regulation and leads to cognitive defects." *Journal of the American Heart Association* 8 (9).

Mukherjee, Avishek, Navid Mohammad Mirzaei, and Pak-Wing Fok. 2024. "Genesis of Intimal Thickening Due to Hemodynamical Shear Stresses." *Mathematical Medicine and Biology.*

Olufsen, M. S. 1999. "A structured tree outflow condition for blood flow in the larger systemic arteries." *American Journal of Physiology* 276: H257-H268.

Olufsen, Mette S., and Ali Nadim. 2004. "On deriving lumped models for blood flow and pressure in the systemic arteries." *Mathematical Biosciences and Engineering* 1 (1).

Pedley, T.J. 2004. "Mathematical modeling of arterial fluid dynamics." *Journal of engineering mathematics* 43 (6): 1239-1245.

Raines, Jeffery K., Michel Y. Jaffrin, and Ascher H. Shapiro. 1974. "A Computer Simulation of Arterial Dynamics in the Human Leg." *Biomechanics* 77 - 91.

Tsao, C.W., Pencina, K.M., Massaro, J.M., Benjamin, E.J., Levy, D., Vasan, R.S., Hoffmann, U., O'Donnell, C.J. and Mitchell, G.F. 2014. "Cross-sectional relations of arterial stiffness, pressure pulsatility, wave reflection, and arterial calcification." *Arteriosclerosis, thrombosis, and vascular biology* 34 (11): 2495-2500.

Van de Vosse, F. N. and Stergiopulos, N. 2011. "Pulse wave propagation in the arterial tree." *Annual Review of Fluid Mechanics* 43: 467-499.

Additional Information

Competing Interests - None of the authors has any conflicts of interests.

Data Availability Statement

The Matlab scripts used to generate the figures in this paper will be made publicly available if this paper is accepted for publication.

Appendix

Characteristic form of Governing Equations

Hyperbolic partial differential equations (PDEs) are conveniently expressed in characteristic form which illustrates the propagation of forward (W_f) and backward (W_b) traveling waves. In terms of characteristic variables, eqs. (1) and (2) become

$$\frac{\partial W_f}{\partial t} + (u+c)\frac{\partial W_f}{\partial x} = H(x) + (u+c)\frac{\partial W_f}{\partial B_0}B_0'(x)$$
$$\frac{\partial W_b}{\partial t} + (u-c)\frac{\partial W_b}{\partial x} = H(x) + (u-c)\frac{\partial W_f}{\partial B_0}B_0'(x)$$

where c is the wave speed, defined as

$$c(A, B_0) = \sqrt{\frac{A}{\rho}\frac{\partial f}{\partial A}}$$

$$H(x) = -\frac{1}{\rho}\frac{\partial f}{\partial B_0}B_0'(x),$$

and $f(A,B_0)$ is the pressure-area tube law from eq. (3). The forward and backward characteristic variables are related to the physical variables u (velocity) and A (lumen area) through

$$W_f = u + \nu(A, B_0)$$
$$W_b = u - \nu(A, B_0)$$

with ν defined by eq. (8).

Hyperelastic Modeling – Derivation of Tube Law

The map from the stress-free reference configuration to the pressurized state is given by r = r(S), with $S_1 < S < S_2$ where S_1 and S_2 are the inner and outer radii of the reference annulus. The hyperelastic energy density is

$$W = \frac{\mu}{2}(I_1 - 3) + \frac{k_1}{2\,k_2}\sum_{n=1}^{2}(e^{k_2 E_n^2} - 1)$$

where I_1 is the first invariant of the Cauchy-Green tensor (see below), μ, k_1 and k_2 are strain energy coefficients and E_n is a strain-like quantity that depends on fibre dispersion; the mathematical definition of E_n can be found in (Jadidi, et al. 2021). The Cauchy stress **T** can be derived from the hyperelastic energy *W* through the relation

$$\boldsymbol{T} = -\gamma \boldsymbol{I} \; + \; 2\boldsymbol{F}\,\frac{\partial W}{\partial \boldsymbol{C}}\boldsymbol{F}^T$$

where γ is a Lagrange multiplier that enforces incompressibility, **F** = diag(r'(S),r/S,1) is the deformation gradient, $\mathbf{C}=\mathbf{F}^{\mathrm{T}}\mathbf{F}$ is the Cauchy-Green tensor, and **I** is the identity tensor. Neglecting wall inertia (Formaggia, Lamponi and Quarteroni 2003), **T** = $\mathrm{diag}(T_{rr}, T_{\theta\theta}, T_{zz})$ satisfies $\nabla \cdot \boldsymbol{T} = 0$. Assuming that the outer boundary is traction-free, and the lumen pressure is *P*, we have the boundary conditions $T_{rr}(S = S_1) = -P$ and $T_{rr}(S = S_2) \; = \; 0$. This leads to

$$P = -\int_{S_1}^{S_2}(T_{rr} \; - \; T_{\theta\theta}) \times \frac{r'(S)}{r(S)}\,dS \equiv f(A, B_0)$$

which results in eq. (9) when written out in full.

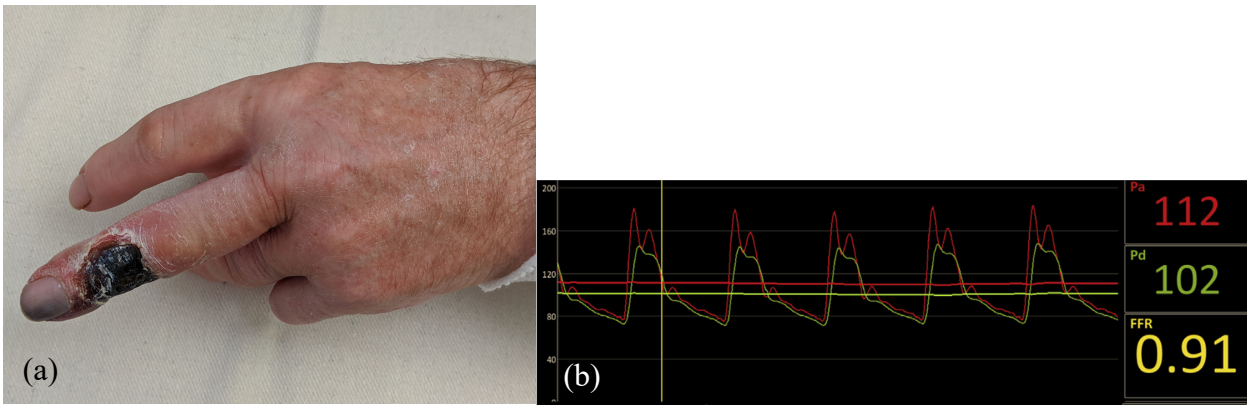

Figure 1: Left - Patients with diabetes or atherosclerosis often have MAC. A decreased flow rate leads to lack of oxygen perfusion in surrounding tissues leading to ischemia and necrosis. Right – High fidelity pressure measurements at mid-brachial (Pa) and distal ulnar (Pd) arteries for a patient with MAC, demonstrating a drop in systolic pressure. The Fractional Flow Reserve (FFR) = 0.91 is diminished due to MAC, despite the lack of atherosclerotic lesions. Taken from (Lanzer, et al. 2021)

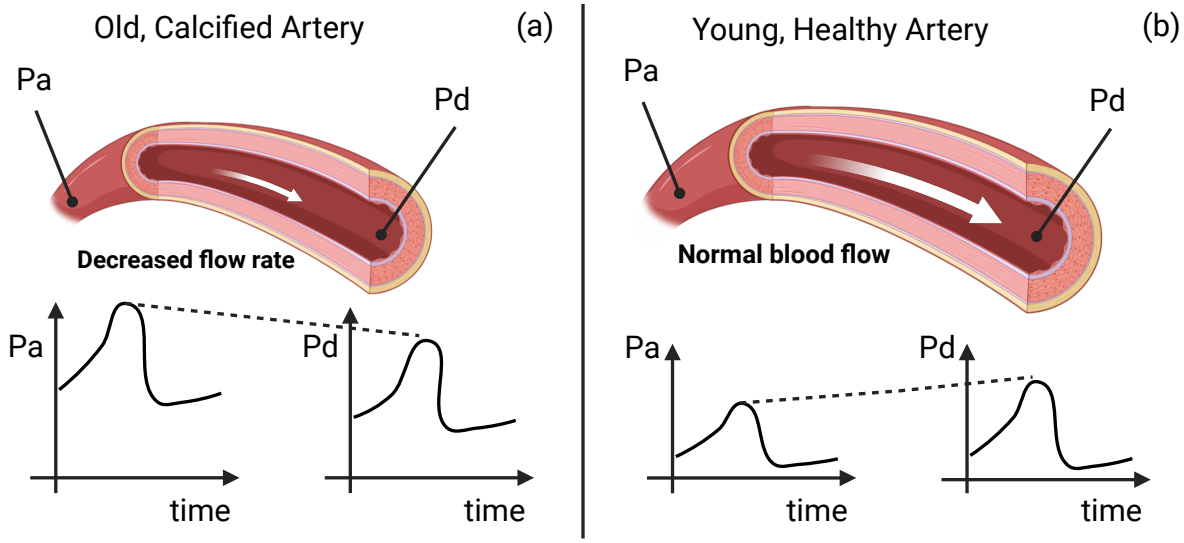

Figure 2: (a) An old, calcified artery suffers a drop in systolic pressure across the artery so that Pa/Pd > 1. (b) A young, healthy artery usually presents an increase in systolic pressure so that Pa/Pd < 1.

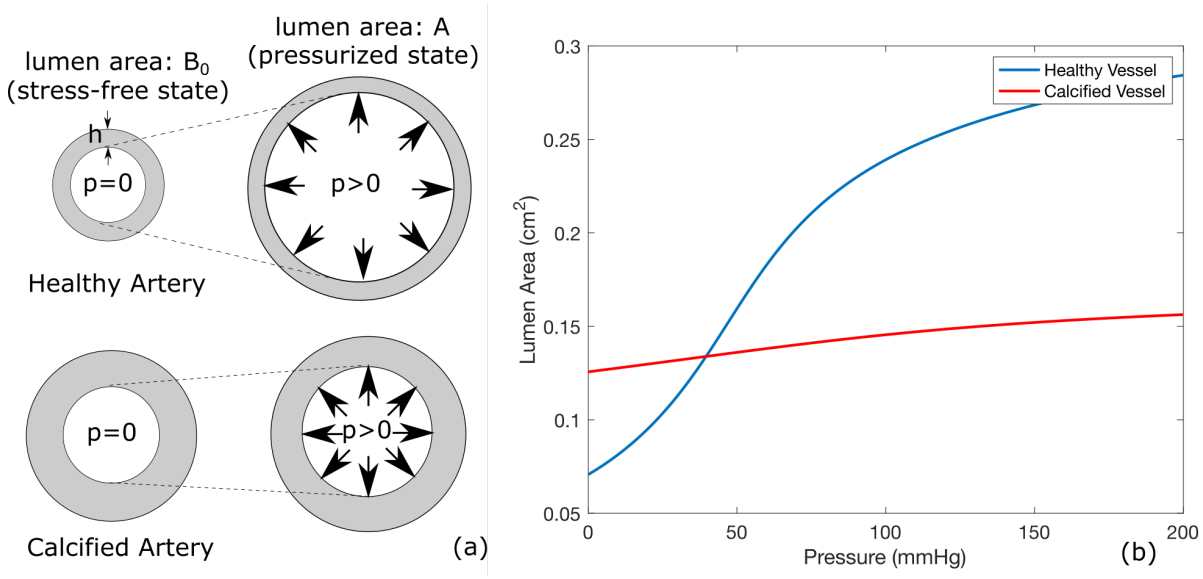

Figure 3: (a) Hyperelastic modeling of healthy and calcified arteries. The lumen areas are B_0 in the stress-free state and expand to A under a pressure p>0. Area and pressure are related through a "tube law" p = f(A,B_0) as given by eq. (3). The law includes the effect of two families of collagen fibres embedded in the arterial wall (not shown). (b) Area-pressure curves for healthy and calcified vessels. Unpressurized dimensions were taken from (Jadidi, et al. 2021).

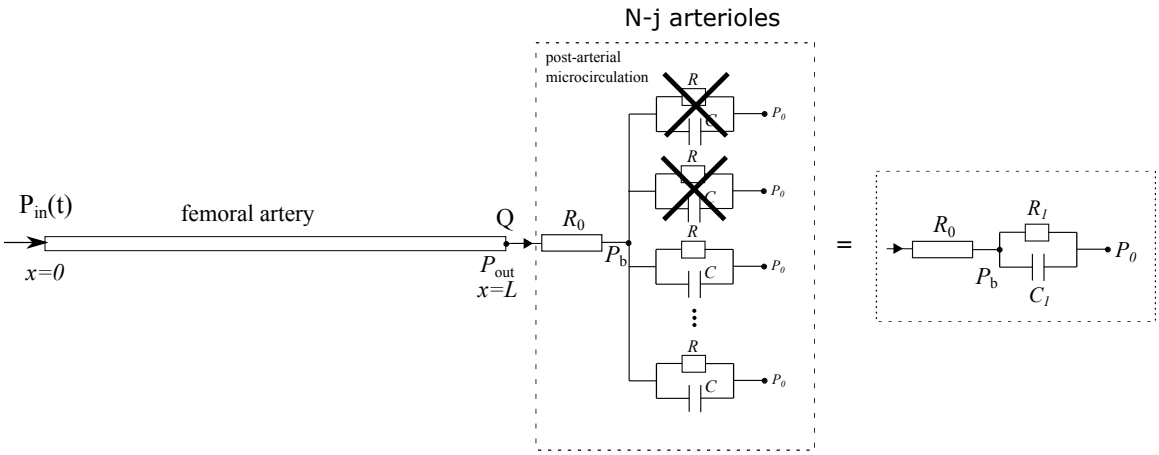

Figure 4: Main variables, parameters, and boundary conditions for hemodynamic simulation in a femoral-popliteal artery. At the inflow x=0, the pressure $P_{in}(t)$ is prescribed. Windkessel elements simulate a post-arterial circulation with N arterioles which gives rise to boundary conditions at x=L. The pressures P_0, P_b and flow rate Q(L,t) evolve in time through equations (5)-(7). In a healthy microcirculation, $R_1 = R_T$ and $C_1 = C_T$. Obstruction of j daughter arterioles in the peripheral circulation results in modified Windkessel parameters $R_1 = R_T/(1-s)$ and $C_1 = C_T(1-s)$ where s = j/N.

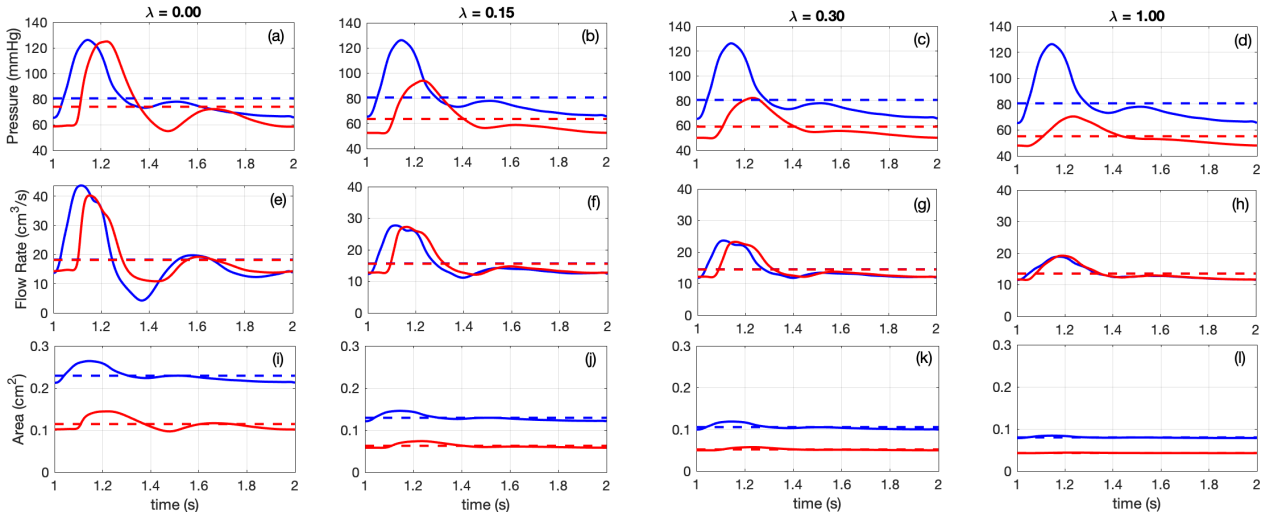

Figure 5: Simulated flow profiles for a healthy ((a), (e), (i)), mildly calcified ((b), (f), j)), moderately calcified ((c), (g), (k)), and severely calcified ((d), (h), (i)) femoral-popliteal arteries. Pressure inlet conditions and peripheral resistances/capacitances were identical for each case (see Table 2).

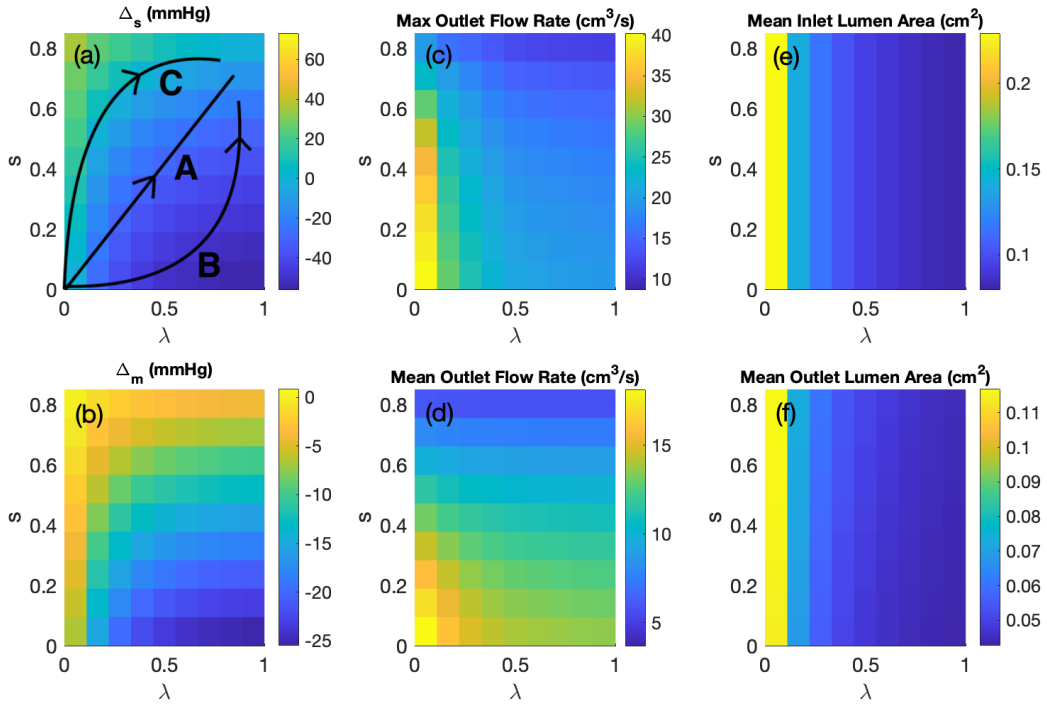

Figure 6: Key hemodynamic quantities as functions of λ (degree of calcification) and s (fraction of closed arterioles). (a) Systolic pressure difference (see eq. (11) for definition), (b) Mean pressure difference (see eq. (12) for definition), (c) Maximum flow rate at arterial outlet, (d) Mean flow rate at arterial outlet, (e) Mean lumen area at inlet, (f) Mean lumen area at outlet. In (a), 3 different calcification-closure pathways are indicated.

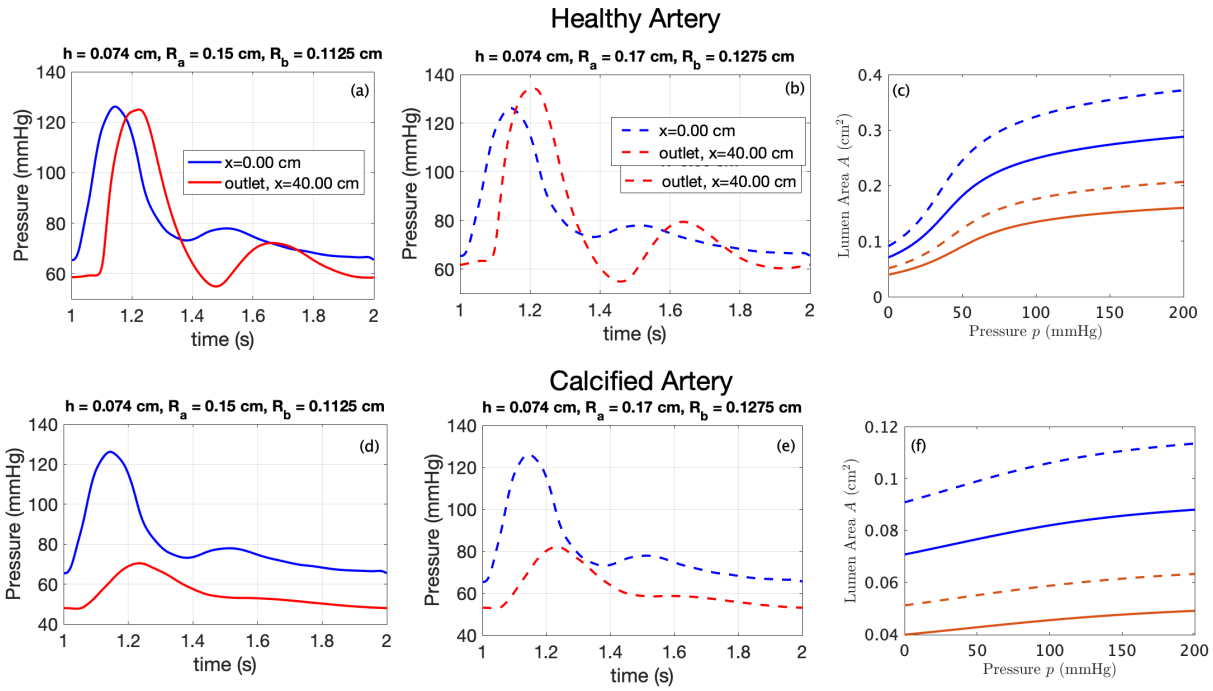

Figure 7: Effect of wall thickening and lumen enlargement on pressure profiles in healthy and calcified arteries. h is the wall thickness, R_a is the unpressurized inlet radius, and $R_b = \zeta \times R_a$ is the unpressurized outlet radius where $\zeta = 0.75$ is the tapering factor. Top row corresponds to a healthy artery (λ=0) while bottom row corresponds to a calcified artery (λ=1). Solid lines correspond to non-remodeled arteries in (a, d) while dashed lines correspond to remodeled arteries in (b, e). (a) and (d) Inlet and outlet pressures for R_a = 0.15 cm, R_b = 0.1125 cm and h = 0.074 cm. (b) and (e) Inlet and outlet pressures for R_a = 0.17 cm, R_b = 0.1275 cm and h = 0.074 cm. (c) and (f) Pressure-Area curves at the inlet (blue, x=0) and outlet (red, x=L).

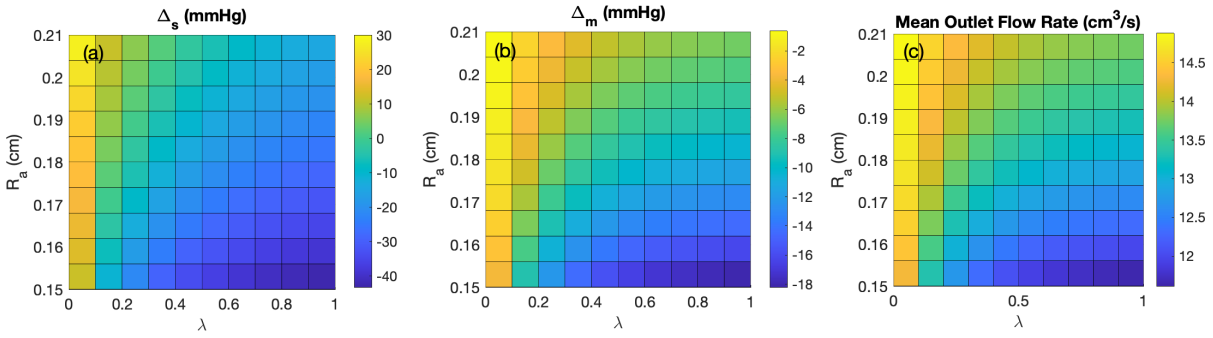

Figure 8: Key hemodynamic quantities as functions of degree of calcification λ and unpressurized lumen radius R_a with s = 0.3 and α = 1. (a) Change in systolic pressure across artery, Δ_s as defined by eq. (11). (b) Change in mean pressure across artery, Δ_m as defined by eq. (12). (c) Time-averaged flow rate at outlet.

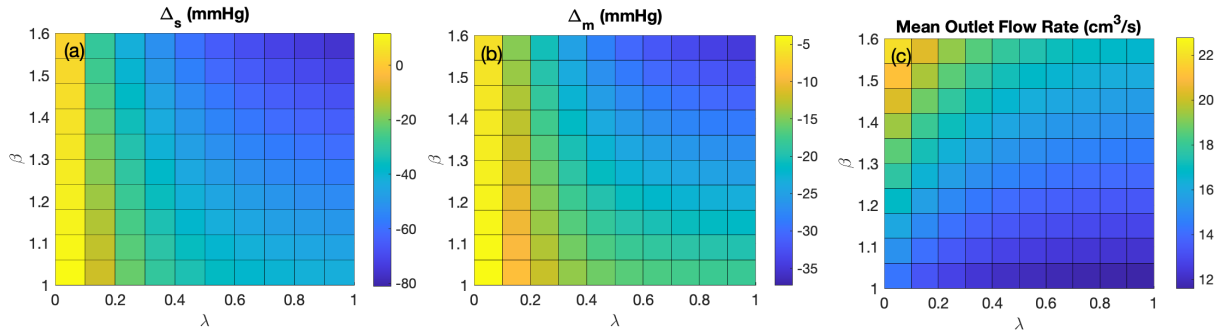

Figure 9: Key hemodynamic quantities as functions of degree of calcification λ and pressure amplification factor β with s = 0.3 and R_a = 0.15 cm. (a) Change in systolic pressure across artery, Δ as defined by eq. (11). (b) Change in mean pressure across artery: a negative value indicates a pressure drop going from inlet to outlet. (c) Mean flow rate at outlet.

Table 1: Mechanical parameters for a healthy and calcified artery. Taken from Patients 2 and 14 of (Jadidi, et al. 2021).

	Symbol	Meaning	Value
Healthy Artery	$\kappa_{ip,H}$	Fibre dispersion parameter	0.12
	$\kappa_{op,H}$	Fibre dispersion parameter	0.39
	ϕ_H	Fibre angle	49°
	μ_H	Strain energy coefficient	114.6 mmHg
	$k_{1,H}$	Strain energy coefficient	86.9 mmHg
	$k_{2,H}$	Strain energy coefficient	3.54 mmHg
Calcified Artery	$\kappa_{ip,C}$	Fibre dispersion parameter	0.13
	$\kappa_{op,C}$	Fibre dispersion parameter	0.47
	ϕ_C	Fibre angle	44°

	μ_C	Strain energy coefficient	894.4 mmHg
	$k_{1,C}$	Strain energy coefficient	649.9 mmHg
	$k_{2,C}$	Strain energy coefficient	171.23 mmHg

Table 2: Geometric and hemodynamical parameters for 1D blood flow simulation.

Symbol	Meaning	Value
L	Length of artery	40 cm
R_0	Resistance in Windkessel element	1.05 mmHg s/cm^3
R_T	Resistance in Windkessel element	3.02 mmHg s/cm^3
C_T	Capacitance in Windkessel element	0.03 cm^3/mmHg
P_{ext}	Hydrostatic blood pressure at t=0	65.5 mmHg
P_0	Terminal pressure for arterioles	0 mmHg
h	Arterial wall thickness (unpressurized)	0.074 cm
ρ	Density of blood	7.5×10^{-4} mmHg s^2/cm^2
R_a	Arterial radius (unpressurized)	0.15 cm
ζ	Tapering factor	0.75
β	Amplification factor for inlet pressure	1 – 1.6

Table 3: Effect of calcification (λ), arteriole closures (s), positive remodeling (R_a) and mean arterial pressure (β) on outlet systolic pressure and mean flow rate.

	Increasing Calcification	More arteriole closures	Positive remodeling	Increasing mean pressure
Outlet Systolic Pressure	Decreases	Increases	Increases	Increases
Mean Flow Rate	Decreases	Decreases	Increases	Increases